THE JOURNAL OF PHYSICAL CHEMISTRY C

Article

Cite This: J. Phys. Chem. C 2019, 123, 4715−4720

pubs.acs.org/JPCC

Modeling Polaron Diffusion in Oligoacene-like Crystals

Marcelo Lopes Pereira, Jr.,[†] Rafael Timóteo de Sousa, Jr.,[‡] Geraldo Magela e Silva,[†] and Luiz Antonio Ribeiro, Jr.*[,†]

[†]Institute of Physics, University of Brasília, Brasília 70910-900, Brazil

[‡]Department of Electrical Engineering, University of Brasília, CP04455, Brasília 70919-970, Brazil

ABSTRACT: Due to the polaronic self-localization of carriers at one or few molecules in organic crystalline semiconductors, the net mobility of a polaron is suppressed and it becomes thermally activated. As a consequence, incoherent hopping of small or large polarons governs the charge transport mechanism, which incorporates crucial contributions of the carriers' diffusion. Here, we develop a model Hamiltonian to theoretically investigate the polaron diffusion as well as its underlying properties in highly ordered two-dimensional arrays of molecules. Our findings show that the polaron diffuses in a typical random-walk motion. Within this transport picture, a critical limit is established for the room temperature diffusivity and activation energy, being the later considerably small. This critical limit for the polaron diffusivity is based on a systematic study of the role of temperature and dimensionality on charge transport with a specific choice of parameters. Moreover, such a low barrier for the activation energy is a straightforward consequence of adopting pristine lattices. We also discuss the polaron stability and mobility as a function of different regimes of the thermal bath. Importantly, these results may provide options to derive the Seebeck coefficient in organic crystalline semiconductors.

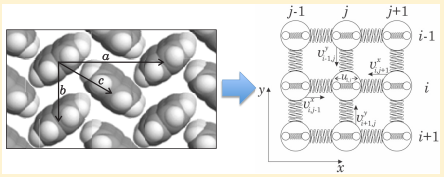

The left panel shows a schematic representation of the two-dimensional herringbone packing in a pentacene crystal and the right panel illustrates our representation for this system.

INTRODUCTION

Organic crystalline semiconductors have emerged as promising candidates to obtain more efficient optoelectronic devices since recent achievements in the photovoltaic technology.[1] Their weak intermolecular van der Waals interactions, combined with the intramolecular and intermolecular degrees of freedom for the electron−lattice interactions, lead them to present particular traits that are desirable to develop a new class of organic-based devices, with a more suitable balance between cost and efficiency than that of their inorganic counterparts. Another interesting application of the organic semiconducting materials due to the growth of the green energy industry is thermoelectric devices.[2,3] In this device, the temperature-induced transport of charge carriers is a crucial issue and should be understood in detail to enhance the thermoelectric figures.

Recently, theoretical efforts have produced relevant outcomes that include characterization methods, devices, and approaches to understand the charge transport mechanism in organic materials.[4−15] Wang, Prezhdo, Beljonne, and their colleagues have studied the major problem of nonadiabatic transport. In this case, more sophisticated dynamical methodologies, such as surface hopping methods, should also be considered.[4−9,11,12] Other research groups have developed a hopping model that describes the charge mobility and can also explain the observed bandlike behavior.[10,13−15] This model uses the Marcus theory coupled with a random-walk simulation of charge diffusion. The studies mentioned above have shed light on the understanding of the overall properties for the charge transport in organic materials. However, a detailed knowledge about the diffusion limit of charge carriers in organic materials, at a molecular level, is lacking in the literature and it can provide options to place the charge transport efficiency in a higher level.

Herein, the diffusion of a polaron in a two-dimensional array of molecules in the framework of Holstein−Peierls Hamiltonian is investigated, that considers both intramolecular and intermolecular electron−lattice interactions. An Ehrenfest molecular dynamics approach is employed using a two-dimensional tight-binding model. This approach allows us to include the temperature effects through the canonical Langevin equation. Importantly, the semiempirical model Hamiltonian is parameterized to resemble single layers in molecular semiconductors such as pentacene[16] and rubrene.[17] Our numerical procedure determines critical limits for the activation energy and diffusivity of a polaron when single layers of these materials are subjected to different thermal baths. Importantly, these critical limits for the polaron diffusivity are based on a systematic study of the role of temperature and dimensionality in charge transport with a specific choice of parameters.

METHODOLOGY

The organic crystalline semiconductors are modeled here by considering a lattice formed of a molecular array where each of its site represents an *i*, *j* molecule, where *i* and *j* index the rows

Received: November 27, 2018
Revised: February 7, 2019
Published: February 11, 2019

DOI: 10.1021/acs.jpcc.8b11459
J. Phys. Chem. C 2019, 123, 4715−4720

(*x*-direction) and columns (*y*-direction), respectively. Alternatively, this two-dimensional array reduces to a stack of molecules, leading, therefore, to a one-dimensional structure. For the sake of convenience, the one-dimensional case will be discussed later to depict the polaron diffusion through the lattice. Figure 1 shows a schematic representation of both the

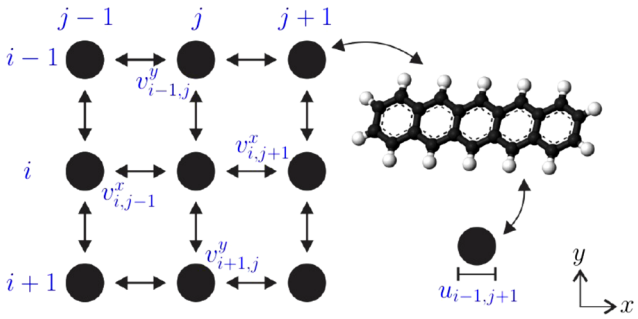

Figure 1. Schematic representation for the model molecular array considered here. In this representation, $v^x_{i,j}$ and $v^y_{i,j}$ denote the relative displacement of a molecule, from its equilibrium position, in *x*- and *y*-directions, respectively. *u* denotes the intrasite displacement of a particular molecule.

one- and two-dimensional structures. In this representation, (v_{n-1} and v_{n+1}) and ($v^x_{i,j}$ and $v^y_{i,j}$) denote the relative displacement of a molecule, from its equilibrium position, for the one- and two-dimensional cases, respectively. In both systems, *u* denotes the intrasite displacement of a particular molecule.

The equations of our model are written using indexes (*i*, *j*), denoting the two-dimensional treatment. For the one-dimensional case, the equations are analogous, excluding the terms in the *y*-direction. Organic molecular crystals are recognized to exhibit two types of electron−phonon couplings: the local intramolecular (Holstein-type[18,19]) and the nonlocal intermolecular (Peierls-type[20]). In this way, our model Hamiltonian combines the Holstein and Peierls approaches as follows

$$H = H_{e,1} + H_{e,2} + H_{l,1} + H_{l,2} \tag{1}$$

where

$$H_{e,1} = \sum_{i,j} \alpha_1 u_{i,j} \hat{c}^\dagger_{i,j} \hat{c}_{i,j} \tag{2}$$

and

$$H_{e,2} = \sum_{i,j} (J^x_{i,j;i,j+1} \hat{c}^\dagger_{i,j+1} \hat{c}_{i,j} + \text{h. c.}) + \sum_{i,j} (J^y_{i,j;i+1,j} \hat{c}^\dagger_{i+1,j} \hat{c}_{i,j} + \text{h. c.}) \tag{3}$$

In this formalism, each site of the lattice has a local intramolecular displacement, $u_{i,j}$, that is coupled to the electronic part of the system by the intramolecular electron−phonon coupling (Holstein parameter), α_1. The intermolecular interactions, in turn, are governed by the electronic transfer integral $J^{x,y}_{i,j;i',j'}$ that couples the electronic and lattice degrees of freedom through an intermolecular electron−phonon coupling term (Peierls parameter), α_2. The overall expression for the electronic transfer integrals reads

$$J^x_{i,j;i,j+1} = J^x_0 - \alpha_1 (v^x_{i,j+1} - v^x_{i,j}) \tag{4}$$

and

$$J^y_{i,j;i+1,j} = J^y_0 - \alpha_2 (v^y_{i+1,j} - v^y_{i,j}) \tag{5}$$

In eqs 4 and 5, J^x_0 and J^y_0 denote the strength of the transfer integral for the *x*- and *y*-directions, respectively, in pristine lattices where the molecules are equally spaced. $\hat{c}^\dagger_{i,j}(\hat{c}_{i,j})$ creates (annihilates) a charge carrier at the (*i*, *j*)-site in the molecular matrix. For the lattice treatment, the system is separated into two harmonic oscillators to account for the contributions of the intra- and intermolecular vibrations, as describe below

$$H_{l,1} = \frac{K_1}{2} \sum_{i,j} (u_{i,j})^2 + \frac{M_1}{2} \sum_{i,j} (\dot{u}_{i,j})^2 \tag{6}$$

and

$$H_{l,2} = \frac{K_2}{2} \sum_{i,j} ((v^x_{i,j+1} - v^x_{i,j})^2 + (v^y_{i+1,j} - v^y_{i,j})^2) + \frac{M_2}{2} \sum_{i,j} ((\dot{v}^x_{i,j})^2 + (\dot{v}^y_{i,j})^2) \tag{7}$$

where K_1 and K_2 are the force constants and M_1 and M_2 are the harmonic oscillator masses. In this notation, as well as for the electronic part, indexes 1 and 2 refer to the intra- and intermolecular terms, respectively. The present study considers only isotropic systems ($J^x_0 = J^y_0$). Table 1 presents the set of parameters employed in the model Hamiltonian. These parameters have been used successfully to model oligoacene-like crystals in other theoretical studies.[21−25]

Table 1. Set of Parameters Used in the Simulations

parameter	value
$J^{x,y}_0$	50.0 meV
α_1	1.8 eV/Å
α_2	0.4 eV/Å
K_1	14.0 eV/Å^2
K_2	0.9 eV/Å^2
M_1	2.88 × 10^{10} eV (as/Å)^2
M_2	5.76 × 10^{10} eV (as/Å)^2

Now, we turn to the equations that govern the dynamics of the system. The electronic dynamics is described by the time-dependent Schrödinger equation (TDSE)

$$i\hbar \psi_k(i, j, t) = (H_{e,1} + H_{e,2}) \psi_k(i, j, t) \tag{8}$$

where $\psi_k(i, j, t)$ is the time-dependent wave function of the two-dimensional system. By introducing instantaneous eigenstates, the solution of the TDSE at each time step, $\Psi(t)$, can be obtained from the one-particle states

$$\psi_k(i, j, t + \Delta t) = \sum_l \left(\sum_{n,p} \phi_l^*(n, p) \psi_k(n, p, t) \right) \times \exp\left(-\frac{i\varepsilon_l \Delta t}{\hbar} \right) \phi_l(i, j) \tag{9}$$

in which $\phi_l(m)$ and ε_l are the instantaneous eigenfunctions and eigenvalues for the electronic part of the Hamiltonian at a time *t*, respectively. Regarding the lattice dynamics, the motion of the molecules is described by Newton's equation for intramolecular displacements obtained from the expectation

DOI: 10.1021/acs.jpcc.8b11459
J. Phys. Chem. C 2019, 123, 4715−4720

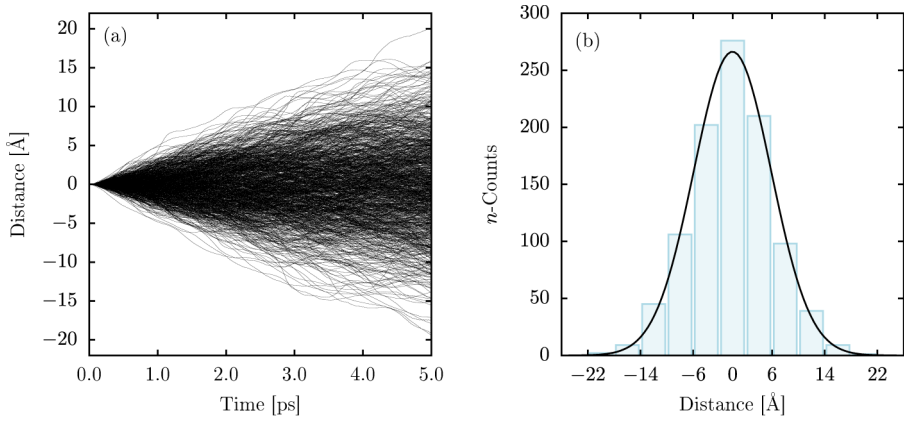

Figure 2. (a) Polaron trajectory for 2000 realizations at 100 K. (b) Distribution of the polaron displacement regarding its initial position at 5 ps.

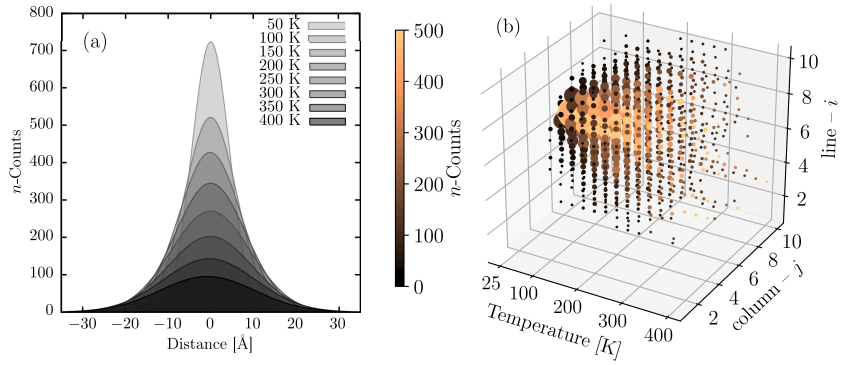

Figure 3. Distribution of the polaron displacement regarding its initial position at 5 ps for (a) a one-dimensional lattice and (b) a two-dimensional lattice.

value of the Lagrangian with respect to the system's wave function

$$F_u \equiv M_1\ddot{u}_{i,j}(t) = -K_1 u_{i,j}(t) - \frac{\alpha_1}{M_1}\rho_{i,j;i,j}(t) \tag{10}$$

and the intermolecular displacements in the x-direction

$$\begin{aligned} F_{v^x} \equiv M_2\ddot{v}^x_{i,j}(t) &= -K_2(2v^x_{i,j}(t) - v^x_{i,j+1} - v^x_{i,j-1}) \\ &-\frac{\alpha_2}{M_2}(\rho_{i,j;i,j-1}(t) - \rho_{i,j;i,j+1}(t)) \\ &-\frac{\alpha_2}{M_2}(\rho_{i,j+1;i,j}(t) - \rho_{i,j-1;i,j}(t)) \end{aligned} \tag{11}$$

and in y-direction

$$\begin{aligned} F_{v^y} \equiv M_2\ddot{v}^y_{i,j}(t) &= -K_2(2v^y_{i,j}(t) - v^y_{i+1,j} - v^y_{i-1,j}) \\ &-\frac{\alpha_2}{M_2}(\rho_{i,j;i-1,j}(t) - \rho_{i,j;i+1,j}(t)) \\ &-\frac{\alpha_2}{M_2}(\rho_{i+1,j;i,j}(t) - \rho_{i-1,j;i,j}(t)) \end{aligned} \tag{12}$$

where $\rho_{i,j;i',j'}(t)$ denotes the electron density matrix that is given by

$$\rho_{i,j;i',j'}(t) = \psi(i, j, t)\psi^*(i', j', t) \tag{13}$$

To consider temperature effects, we use the Langevin formalism within the scope of the Brünger−Brooks−Karplus method.[26] Here, we use thermal random forces from a Gaussian distribution, with zero mean value, $\langle\zeta(t)\rangle \equiv 0$, and variances

$$\langle R^{\text{intra}}_{i,j}(t)R^{\text{intra}}_{i',j'}(t')\rangle \equiv 2k_B T M_1\lambda_1\delta_{i,j;i',j'}\delta(t - t') \tag{14}$$

and

$$\langle R^{\text{inter}}_{i,j}(t)R^{\text{inter}}_{i',j'}(t')\rangle \equiv 2k_B T M_2\lambda_2\delta_{i,j;i',j'}\delta(t - t') \tag{15}$$

To keep the temperature constant after a transient period, it is necessary to include damping constants for the intra- and intermolecular motions, with constants λ_1 and λ_2, respectively. These parameters are settled as 5.0×10^4 as^{-1}. In this way, we can derive the new equations for the lattice dynamics as follows

$$F'_u \equiv F_u - M_1\lambda_1\dot{u}_{i,j} + R^{\text{intra}}_{i,j}(t) \tag{16}$$

$$F'_{v^x} \equiv F_{v^x} - M_2\lambda_2\dot{v}^x_{i,j} + R^{\text{inter}}_{i,j}(t) \tag{17}$$

and

$$F'_{v^y} \equiv F_{v^y} - M_2\lambda_2\dot{v}^y_{i,j} + R^{\text{inter}}_{i,j}(t) \tag{18}$$

RESULTS

We begin the discussion of the results by presenting the polaron diffusion in a one-dimensional lattice with 100 molecules, subjected to different thermal baths. Figure 2 illustrates the polaron propagation (Figure 2a) and final position (Figure 2b) for 2000 realizations at 100 K. The lines in Figure 2a represent the polaron position as a function of time for a given realization, i.e., a seed for the random number

DOI: 10.1021/acs.jpcc.8b11459
J. Phys. Chem. C 2019, 123, 4715−4720

generator used in the Langevin dynamics. It is worth mentioning that the details about the geometric and dynamical properties of the polaron in molecular crystals were already studied.[23] Moreover, the polaron position in the lattice at a given time step follows the expression given in ref 20. Here, the distance between the molecules is 3.5 Å. In Figure 2a, one can realize that the polaron is evolving in time in the typical Brownian motion. The fluctuations along the polaron trajectory are a signature of the temperature effects. As presented in the previous section, the thermal effects enter in the lattice part of the model in such a way that the vibrations of the molecules can transfer energy to the polaron, leading to displacements in its position due to the presence of electron−lattice interactions. This physical picture fits in the scope of the Wiener process. Furthermore, there is a clear dispersion trend of the polaron path, which suggests a diffusive behavior. The counting of the polaron's final position, i.e., its displacement regarding the origin, is useful to understand the critical limit for the polaron diffusion in a particular lattice. In this way, Figure 2b displays the polaron distribution regarding the distance from the origin during 5 ps of simulation. Such an analysis can be used to derive the probability of finding a polaron at a region in the lattice. The Gaussian regression in Figure 2b clearly shows that the average position for the polaron displacement is zero, as expected due to the symmetry of the system.

It is worth discussing here the distribution of the polaron position in one- and two-dimensional lattices when subjected to different thermal baths. In this way, Figure 3a,b presents the counting for the polaron's final position in one- and two-dimensional systems, respectively. The one-dimensional system is a 100 × 1 lattice (100 molecules), whereas the two-dimensional one is a 10 × 10 matrix (100 molecules). In this way, for the sake of comparison, both systems have the same total number of molecules. In both cases, one can note that for higher temperatures the polaron delocalization increases. Consequently, the counting for the zero displacement decreases proportionally. In Figure 3b, the polaron position is represented by circles of different sizes and colors. The polaron positions follow the matrix notation according to Figure 1. In this scheme, the bigger circles represent higher values of counting, whereas small circles denote the opposite. The color scale helps in identifying the regions where the counting for the polaron displacement possesses high value. Albeit not shown here, it is important to mention that the polaron diffusion in the two-dimensional systems also presents a characteristic behavior of a Wiener process. These results suggest that the temperature-mediated polaron dispersion in organic molecular crystals is limited to around ten molecules. Since the model crystals employed here are pristine lattices, such a critical limit for the polaron diffusion in real systems should be, in fact, considerably smaller. Some internal and external processes such as lattice defects[27] and charge recombination[28] may contribute to lower the polaron's mean free path in these materials.

Now we can turn to the discussion about the polaron stability and mobility in lattices subjected to a thermal bath. To do so, Figure 4 shows the typical time evolution of the mean-square displacement for the polaron trajectories depicted in Figure 2a. The red dots establish the linear regression over 2000 realizations. From the angular coefficient of this regression, it is possible to evaluate the polaron diffusivity

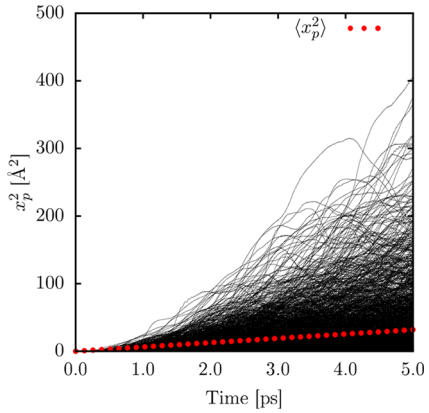

Figure 4. Time-dependent squared displacement for the polaron transport in a one-dimensional lattice.

$$D = \frac{1}{2n}\lim_{t\to\infty}\frac{\langle x_p^2\rangle}{t} \tag{19}$$

where n is the space dimension. Then, the mobility of the polaron can be calculated using the Einstein relationship

$$\mu = \frac{e}{k_B T}D \tag{20}$$

The temperature-dependent transport of polarons in organic molecular crystals is typical of a mass diffusion process in solids and follows an Arrhenius-type law

$$D(T) = D_0 \exp(-E_A/k_B T) \tag{21}$$

where D_0 is the maximum diffusion coefficient and E_A is the activation energy for the diffusion. We have performed a regression for the polaron diffusivity as a function of the temperature (see Figure 5) using the expression above. This

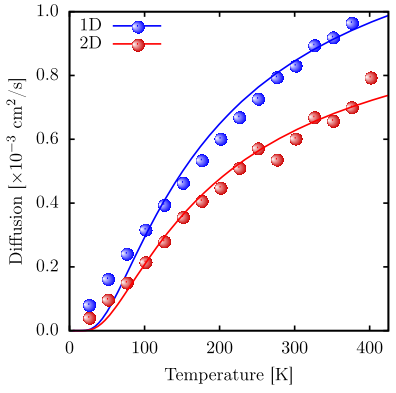

Figure 5. Temperature-dependent polaron diffusivity for (a) one-dimensional and (b) two-dimensional lattices.

regression yields $D_0 = 1.4 \times 10^{-3}$ cm^2/s and $E_A = 12.36$ meV for the one-dimensional system and $D_0 = 1.1 \times 10^{-3}$ cm^2/s and $E_A = 14.31$ meV for the two-dimensional case. The calculated diffusivities are about an order of magnitude higher than the values reported in the literature,[29] and the activation energies are substantially small, a consequence of adopting pristine lattices. Therefore, these results suggest that 1.4×10^{-3} cm^2/s is the limit of diffusivity in organic molecular crystals, as the simulated model lattices are free of disorder or impurities. An explanation for the higher diffusivity (and mobility) in one-

DOI: 10.1021/acs.jpcc.8b11459
J. Phys. Chem. C 2019, 123, 4715−4720

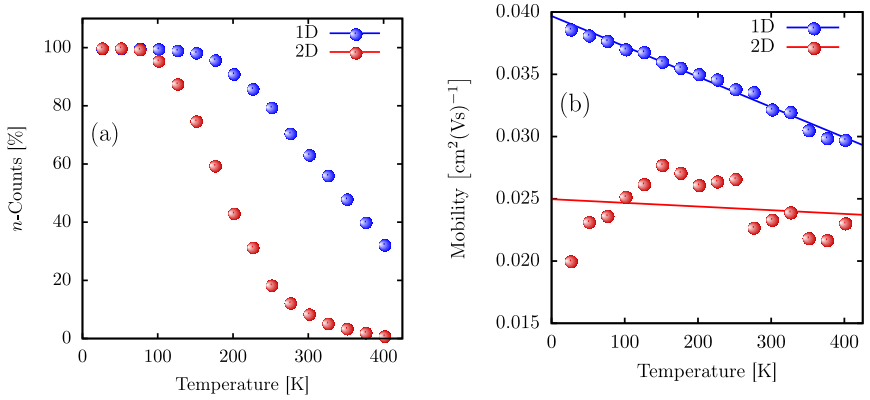

Figure 6. Temperature-dependent (a) polaron stability and (b) mobility.

dimensional stacks will be presented below. To quantitatively understand the polaron stability, in turn, the inverse participation ratio (IPR) for the charge density is used, according to that established in ref 24.

Since mobility calculations are performed only for realizations where stable polarons are present, it is interesting to discuss first the polaron stability as a function of the temperature. To do so, we use the average value of the inverse participation ratio (IPR) as a measurement for the polaron integrity.[24] A throughout discussion on IPR usefulness can be found in ref 30. The IPR is derived with respect to the molecular charge density. This quantity is a measure of the number of sites that share the charge and is defined as

$$\mathrm{IPR} = \frac{\sum_i |\rho_{i,j}|^4}{\sum_i (|\rho_{i,j}|^2)^2} \tag{22}$$

IPR values close to zero denote systems in which the polaron is not stable. If the IPR lies in the range of 0.2−0.4, a metastable polaron solution is obtained. For IPR values between 0.4 and 0.8, the charge is usually shared by five molecules and the resulting carrier is named large polaron. Finally, IPR values greater than 0.8 refer to solutions in which the molecular charge is localized in one molecule, resulting in a carrier that is termed small polaron. The $\overline{\mathrm{IPR}}$ is calculated using the IPR values obtained at each time step during the last 2 ps, neglecting, therefore, the initial polaron configuration that is equal for all realizations. This procedure is adopted to obtain a better insight into the impact of different thermal baths on the dynamical stability of the polaron. $\overline{\mathrm{IPR}}$ values greater than 0.4 represent a stable polaron solution, and the *n*-counts in Figure 6a denote, in percentage terms, the amount of realizations in which $\overline{\mathrm{IPR}}$ is greater than this critical value. In this way, Figure 6a presents the percentage count of stable polarons over 2000 realizations in one- and two-dimensional lattices, blue and red circles, respectively, for different thermal baths ranging in the interval 25−400 K with an increment of 25 K. From this figure, one can note that polarons tend to be more dynamically stable when it comes to one-dimensional lattices. The reason for this trend is the reduction in the number of degrees of freedom for the lattice vibrations in the one-dimensional case when compared with the two-dimensional one. Since molecular vibrations can delocalize the charge coupled to a particular molecule, high temperatures increase the energy associated with the molecular vibrations. This energy, therefore, is transferred to the polaronic charge due to the electron−lattice interaction, increasing, consequently, the charge displacement. When this displacement reaches a critical limit, the mutual interaction between charge and lattice deformations that characterizes the polaron becomes energetically prohibitive, leading to the process of loss of stability. Note that a molecule in the two-dimensional system is surrounded by four intermolecular oscillators, whereas in the one-dimensional case, there are just two neighboring oscillators (see Figure 1).

The degree of stability of the polaron in the different lattices reflects directly the trend obtained for its mobility. Figure 6b illustrates the temperature-dependent polaron mobility (an average over 2000 realizations) for both one- and two-dimensional lattices. The blue and red lines represent the regression for the respective data set. It is worth noticing that intrinsic charge mobility is difficult to obtain once it depends, for example, on the conditions of material fabrication. Nevertheless, these theoretical results can provide reference values. In Figure 6b, one can note that the polaron mobility (and diffusivity, see Figure 5) is higher for the one-dimensional case. This is a straightforward consequence of the polaronic effective mass that is smaller in the one-dimensional lattice. The fluctuations in the average mobility values presented for the two-dimensional case are a consequence of the reduced sample of stable polarons, which substantially decrease for higher thermal baths. As mentioned above, in such circumstances, the intermolecular phonon scatterings play an appreciable role in delocalizing the polaronic charge by lowering its stability.

The differences in the values obtained for the polaron mobilities in one- and two-dimensional cases are related to the effective mass of the polaron. This underlying polaron property changes with the system's dimensionality, within the scope of our approach, as well discussed in one of our previous research studies.[23] For two-dimensional systems, the stable polaron extends over three molecules on the same row and also over two molecules on neighboring rows, as represented in Figure 1. The difficulties in transferring the two-dimensional polaron from one molecule to the next are due to the fact that all of the distortions in the molecular array associated with the presence of the charge have to be transferred at once from one column to the next. In this sense, more lattice distortions should be transported with the charge in the two-dimensional case regarding the one-dimensional system, which decreases the polaron mobility in the former.

DOI: 10.1021/acs.jpcc.8b11459
J. Phys. Chem. C 2019, 123, 4715−4720

CONCLUSIONS

In summary, the temperature-dependent polaron dynamics was studied in organic semiconductors at a molecular level. Through a systematic numerical approach, a critical limit for the polaron diffusivity was established to be approximately 1.4×10^{-3} cm^2/s. It is worth mentioning that this critical limit for the polaron diffusivity is based on a systematic study of the role of temperature and dimensionality in charge transport with a specific choice of parameters. Moreover, such a critical regime obtained for the model system employed here is expected to be substantially higher than that for real devices, as only pristine lattices are considered in this study. Remarkably, the calculated mobilities are in good agreement with experimental and other theoretical results reported in the literature for the hole and electron mobilities in ordered and disordered molecular crystals. Since intrinsic charge mobilities are very difficult to obtain experimentally, our theoretical results may provide guidance as reference values for other studies.

AUTHOR INFORMATION

Corresponding Author

*E-mail: ribeirojr@unb.br.

ORCID

Luiz Antonio Ribeiro, Jr.: 0000-0001-7468-2946

Notes

The authors declare no competing financial interest.

ACKNOWLEDGMENTS

The authors gratefully acknowledge the financial support from Brazilian Research Councils CNPq, CAPES, and FAP-DF and CENAPAD-SP for providing the computational facilities. This research work has the support of the Brazilian Ministry of Planning, Development and Management (Grants 005/2016 DIPLA, Planning and Management Directorate, and 11/2016 SEST, State-owned Federal Companies Secretariat) and the DPGU, Brazilian Union Public Defender (Grant 066/2016). L.A.R. and G.M.e.S. gratefully acknowledge the financial support from FAP-DF grants 0193.001.511/2017 and 0193.001766/2017, respectively.

REFERENCES

(1) Ostroverkhova, O. Organic Optoelectronic Materials: Mechanisms and Applications. *Chem. Rev.* **2016**, *116*, 13279−13412.
(2) Chen, Y.; Zhao, Y.; Liang, Z. Solution Processed Organic Thermoelectrics: Towards Flexible Thermoelectric Modules. *Energy Environ. Sci.* **2015**, *8*, 401−422.
(3) Bubnova, O.; Khan, Z. U.; Malti, A.; Braun, S.; Fahlman, M.; Berggren, M.; Crispin, X. Optimization of the Thermoelectric Figure of Merit in the Conducting Polymer Poly(3,4-ethylenedioxythiophene). *Nat. Mater.* **2011**, *10*, 429−433.
(4) Wang, L.; Sifain, A. E.; Prezhdo, O. V. Fewest Switches Surface Hopping in Liouville Space. *J. Phys. Chem. Lett.* **2015**, *6*, 3827−3833.
(5) Wang, L.; Akimov, A.; Prezhdo, O. V. Fewest Switches Surface Hopping in Liouville Space. *J. Phys. Chem. Lett.* **2016**, *7*, 2100−2112.
(6) Wang, L.; Prezhdo, O. A Simple Solution to the Trivial Crossing Problem in Surface Hopping. *J. Phys. Chem. Lett.* **2014**, *5*, 713−719.
(7) Wang, L.; Beljonne, D. Flexible Surface Hopping Approach to Model the Crossover from Hopping to Band-like Transport in Organic Crystals. *J. Phys. Chem. Lett.* **2013**, *4*, 1888−1894.
(8) Wang, L.; Olivier, Y.; Prezhdo, O. V.; Beljonne, D. Maximizing Singlet Fission by Intermolecular Packing. *J. Phys. Chem. Lett.* **2014**, *5*, 3345−3353.
(9) Wang, L.; Trivedi, D.; Prezhdo, O. V. Global Flux Surface Hopping Approach for Mixed Quantum-Classical Dynamics. *J. Chem. Theory Comput.* **2014**, *10*, 3598−3605.
(10) Wang, L.; Nan, G.; Yang, X.; Peng, Q.; Li, Q.; Shuai, Z. Computational methods for design of organic materials with high charge mobility. *Chem. Soc. Rev.* **2010**, *39*, 423−434.
(11) Qiu, J.; Bai, X.; Wang, L. Crossing Classified and Corrected Fewest Switches Surface Hopping. *J. Phys. Chem. Lett.* **2018**, *9*, 4319−4325.
(12) Bai, X.; Qiu, J.; Wang, L. An efficient solution to the decoherence enhanced trivial crossing problem in surface hopping. *J. Chem. Phys.* **2018**, *148*, No. 104106.
(13) Nan, G.; Yang, X.; Wang, L.; Shuai, Z.; Zhao, Y. Nuclear tunneling effects of charge transport in rubrene, tetracene, and pentacene. *Phys. Rev. B* **2009**, *79*, No. 115203.
(14) Shuai, Z.; Wang, L.; Li, Q. Evaluation of Charge Mobility in Organic Materials: From Localized to Delocalized Descriptions at a First-Principles Level. *Adv. Mater.* **2011**, *23*, 1145−1153.
(15) Wang, L.; Li, Q.; Shuai, Z.; Chen, L.; Shi, Q. Multiscale study of charge mobility of organic semiconductor with dynamic disorders. *Phys. Chem. Chem. Phys.* **2010**, *12*, 3309−3314.
(16) Coropceanu, V.; Cornil, J.; da Silva Filho, D. A.; Olivier, Y.; Silbey, R.; Brédas, J. L. Charge Transport in Organic Semiconductors. *Chem. Rev.* **2007**, *107*, 926−952.
(17) Troisi, A. Charge Transport in High Mobility Molecular Semiconductors: Classical Models and New Theories. *Chem. Soc. Rev.* **2011**, *40*, 2347−2358.
(18) Holstein, T. Studies of polaron motion: Part I. The molecular-crystal model. *Ann. Phys.* **1959**, *8*, 325−342.
(19) Holstein, T. Studies of polaron motion: Part II. The small-polaron. *Ann. Phys.* **1959**, *8*, 343−389.
(20) Stafström, S. Electron Localization and the Transition from Adiabatic to Nonadiabatic Charge Transport in Organic Conductors. *Chem. Soc. Rev.* **2010**, *39*, 2484−2499.
(21) Mozafari, E.; Stafström, S. Polaron Stability in Molecular Crystals. *Phys. Lett. A* **2012**, *376*, 1807−1811.
(22) Mozafari, E.; Stafström, S. Polaron Dynamics in a Two-Dimensional Holstein-Peierls System. *J. Chem. Phys.* **2013**, *138*, 184104−7.
(23) Ribeiro, L. A. R., Jr.; Stafström, S. Polaron Stability in Molecular Semiconductors: Theoretical Insight into the Impact of the Temperature, Electric Field and the System Dimensionality. *Phys. Chem. Chem. Phys.* **2015**, *17*, 8973−8982.
(24) Ribeiro, L. A., Jr.; Stafström, S. Impact of the Electron-Phonon Coupling Symmetry on the Polaron Stability and Mobility in Organic Molecular Semiconductors. *Phys. Chem. Chem. Phys.* **2016**, *18*, 1386−1391.
(25) Ribeiro, L. A., Jr.; Stafström, S. Polaron Dynamics in Anisotropic Holstein-Peierls Systems. *Phys. Chem. Chem. Phys.* **2017**, *19*, 4078−4084.
(26) Izaguirre, J. A.; Catarello, D. P.; Wozniak, J. M.; Skell, R. D. Langevin Stabilization of Molecular Dynamics. *J. Chem. Phys.* **2001**, *114*, 2090−2098.
(27) de Oliveira Neto, P. H.; da Cunha, W. F.; e Silva, G. M. Charge Carrier Untrapping by Temperature Effects in Conjugated Polymers. *Europhys. Lett.* **2009**, *88*, No. 67006.
(28) da Cunha, W. F.; Ribeiro, L. A., Jr.; Garganoa, R.; e Silva, G. M. Critical Temperature and Products of Intrachain Polaron Recombination in Conjugated Polymers. *Phys. Chem. Chem. Phys.* **2014**, *16*, 17072−17080.
(29) Kadashchuk, A.; Tong, F.; Janneck, R.; Fishchuk, I. I.; Mityashin, A.; Pavlica, E.; Kohler, A.; Heremans, P.; Rolin, C.; Bratina, G.; Genoe, J. Role of Transport Band Edge Variation on Delocalized Charge Transport in High-Mobility Crystalline Organic Semiconductors. *Phys. Rev. B* **2017**, *96*, No. 125202.
(30) Pereira, M. L., Jr.; de Sousa, R. T., Jr.; e Silva, G. M.; Ribeiro, L. A., Jr. Stationary polaron properties in organic crystalline semiconductors. *Phys. Chem. Chem. Phys.* **2019**, *21*, 11−12.

DOI: 10.1021/acs.jpcc.8b11459
J. Phys. Chem. C 2019, 123, 4715−4720